European Conference on Computational Fluid Dynamics
ECCOMAS CFD 2006
P. Wesseling, E. Oñate and J. Périaux (Eds)

PROBABILISTIC MODEL OF UNCERTAINTIES IN TWO-PHASE FLOW TROUGH POROUS MEDIA

Olivier P. Le Maître* **and Christian Soize†**

*Université d'Evry Val d'Essonnne, LMEE
4, rue du Pelvoux, CE 1455, 91 020 Evry cedex, France
e-mail: olm@iup.univ-evry.fr

†Université de Marne la Vallée, LAM, Cité Descartes, Marne la Vallée, France.
e-mail: soize@univ-mlv.fr

Key words: Fluid Flow, Uncertainty, Non-Parametric, Monte-Carlo

Abstract. *We present a probabilistic model of uncertainties for the two-phase flow through a porous medium. The uncertainty in the model comes from an incomplete knowledge of the saturation-dependent effective mobilities of the phases, which are consequently considered as random processes. The probability laws of these processes are derived following the maximum entropy principle. After discretization, the random effective mobilities can be sampled allowing for Monte-Carlo simulations of the random model and analysis of the resulting random flow.*

1 INTRODUCTION

In the last years, uncertainty quantification in fluid flow simulations has considerably developed in response to more and mode concerns regarding the exploitation and interpretation of numerical results[1]. These developments were essentially made possible by the introduction of efficient numerical procedures as the stochastic finite element method[2] and Polynomial-Chaos type expansions in CFD models[3,4,5], allowing for compact representations of uncertainty using a limited number of orthogonal modes. However, these techniques are limited to the propagation of data (parametric) uncertainties in a fixed flow model and so can not deal with model uncertainties. In fact, the analysis of model uncertainty requires a non-parametric approach[6] that to our knowledge remains to be developed in the context of fluid flow simulations.

In this paper, we present a preliminary attempt toward the development of non-parametric techniques for the analysis of uncertainty in fluid flow models. A simple one-dimensional, capillarity-free, incompressible two-phase flow in a porous medium with perfectly known porosity and permeability is considered. The governing equations for this flow are given in section 2. These equations consist of the mass conservation equation and two constitutive relations prescribing the relationships between the effective mobilities and the saturations of the respective phases. The model uncertainty arises from

an incomplete knowledge of the effective mobilities which are consequently considered as random processes. In section 3, the maximum entropy principle is invoked to derive the least informative probability laws of the effective mobilities of the fluids, from the available information and assumptions on the stochastic model. In section 4, a finite dimensional discretization of the effective mobilities is introduced, based on quadratic shape-preserving splines, and a numerical procedure is proposed for the determination of the probability laws of the discretized effective mobilities. Whence these probability laws are found out, they can be sampled to generate realizations of the random flow model, allowing for a Monte-Carlo analysis of the uncertainty impact on the solution. This type of analysis is presented in section 5. Finally, principal findings and major conclusions from this work are reported in section 6, together with possible improvements.

2 TWO-PHASE FLOW MODEL

2.1 Conservative equations

As a preliminary attempt toward non-parametric analysis of model uncertainties in fluid flow simulations, we restrict ourselves to the 1-D, capillarity free, incompressible two-phase flow in a porous medium. The porosity ϕ and absolute permeability a of the medium are certain and uniform through the domain $\Omega = [z^-, z^+] \subset \mathbb{R}$. The mass conservation equations for the two phases ($l = 1, 2$) are :

$$\forall z \in \Omega \ : \begin{cases} \phi \dfrac{\partial s^{(l)}}{\partial t} + \dfrac{\partial \psi^{(l)}}{\partial z} = 0 & l = 1, 2 \\ \psi^{(l)} = -\lambda^{(l)} \left(\dfrac{\partial p}{\partial z} - g^{(l)} \right) & l = 1, 2 \\ s^{(1)} + s^{(2)} = 1. \end{cases} \tag{1}$$

In Eq. 1, $s^{(l)} \in [0, 1]$ is the saturation (or phase's fraction), $\psi^{(l)}$ is the Darcy velocity, p is the pressure, $g^{(l)}$ the gravity term and $\lambda^{(l)} \equiv a k^{(l)}$ is the effective mobility with $k^{(l)}(s^{(l)})$ the saturation dependent mobility of phase l. Introducing $q = \psi^{(1)} + \psi^{(2)}$ the total Darcy's velocity (which is constant in space for an incompressible 1-D flow) the pressure can be easily eliminated from the expressions of the Darcy's velocities to obtain

$$\psi^{(1)} = \frac{\lambda^{(1)}}{\lambda^{(1)} + \lambda^{(2)}} \left[q + (g^{(1)} - g^{(2)}) \lambda^{(2)} \right], \quad \psi^{(2)} = \frac{\lambda^{(2)}}{\lambda^{(1)} + \lambda^{(2)}} \left[q + (g^{(1)} - g^{(2)}) \lambda^{(1)} \right]. \tag{2}$$

Setting $s \equiv s^{(1)}$ and the flux $f \equiv \psi^{(1)}$ the mass conservation becomes

$$\phi \frac{\partial s}{\partial t} + \frac{\partial f}{\partial z} = 0, \quad f = \frac{\lambda^{(1)}}{\lambda^{(1)} + \lambda^{(2)}} \left[q + (g^{(1)} - g^{(2)}) \lambda^{(2)} \right]. \tag{3}$$

To solve Eq. (3), initial and boundary conditions are required. We shall consider that the flow takes place in a domain bounded by impermeable boundaries at $z = z^{\pm}$; boundary

and initial conditions are then

$$\begin{cases} f(z=z^{\pm},t)=0, & \forall t, \\ s(z,t=0)=s_0(z)\in[0,1], & \forall z\in\Omega. \end{cases} \tag{4}$$

Eq. (3) has also to be supplemented with constitutive relations prescribing the effective mobilities $\lambda^{(1)}(s)$ and $\lambda^{(2)}(s)$. As a result, the full model consists of the mass conservation (Eq. (3)), initial and boundary conditions (Eqs. (4)) and the two effective mobilities $\lambda^{(l)}$ for $l=1,2$.

It can be shown that if $s\mapsto\lambda^{(1)}(s)$ (resp. $s\mapsto\lambda^{(2)}(s)$) is an increasing function of s (resp. decreasing), and assuming $g^{(1)}>g^{(2)}$ (*i.e.* fluid 1 is heavier), then the flux $f(s)$ has a unique maximum at a saturation denoted θ :

$$\theta\equiv\arg\max_{s\in[0,1]} f(s). \tag{5}$$

2.2 Solvability condition

The mass conservation equations for the two phases are combines leading to an elliptic equation for the pressure,

$$\frac{\partial}{\partial z}\left[(\lambda^{(1)}+\lambda^{(2)})\frac{\partial p}{\partial z}\right]=g^{(1)}\frac{\partial\lambda^{(1)}}{\partial z}+g^{(2)}\frac{\partial\lambda^{(2)}}{\partial z}. \tag{6}$$

For impermeable walls ($q=0$), the pressure boundary conditions are

$$\frac{\partial p}{\partial z}=\frac{\lambda^{(1)}g^{(1)}+\lambda^{(2)}g^{(2)}}{\lambda^{(1)}+\lambda^{(2)}},\quad z=z^{\pm}. \tag{7}$$

This pressure equation is solvable and has a unique solution (up to an additive constant) if and only if $\lambda^{(1)}+\lambda^{(2)}>0$ for all $z\in\Omega$. Alternatively, valid constitutive relations must satisfy the constraint :

$$0<\max_{s\in[0,1]}\left[\frac{1}{\lambda^{(1)}(s)+\lambda^{(2)}(s)}\right]<+\infty. \tag{8}$$

2.3 Numerical method

Eq. (3) is solved using a classical cell-centered finite volume discretization. The domain Ω is divided into N_z cells with constant size $h=(z^+-z^-)/N_z$. We denote $z_{i+1/2}=z^-+ih$, for $i=0,\ldots,N_z$, the position of the cells' interfaces. A cell with index i corresponds to $z\in[z_{i-1/2},z_{i+1/2}]$. Let $\widehat{s}_i$ be the saturation spatially averaged over the cell with index i :

$$\widehat{s}_i=\frac{1}{h}\int_{z_{i-1/2}}^{z_{i+1/2}} s(z)dz. \tag{9}$$

A first order conservative discretization of Eq. (3) is

$$\phi \frac{\widehat{s}_i^{n+1} - \widehat{s}_i^n}{\Delta t} + \frac{1}{h}\left(f_{i+1/2}^n - f_{i-1/2}^n\right) = 0, \tag{10}$$

where the superscripts refer to the time index. In Eq. (10) the numerical fluxes are expressed as $f_{i+1/2} = g(\widehat{s}_i, \widehat{s}_{i+1})$, where the function $(x, y) \mapsto g(x, y)$ is the solution of a Riemann problem satisfying the following conditions :

- consistency : $g(x, x) = f(x)$,
- monotonicity : $g(x, y)$ increasing (resp. decreasing) with x (resp. with y),
- Lipschitz continuity.

Following Jaffré[7], we use the Godunov's flux

$$g(\widehat{s}, \widehat{s}') \equiv \min\left[f\left(\min\{\widehat{s}, \theta\}\right), f\left(\max\{\theta, \widehat{s}\}\right)\right], \quad f = \frac{\lambda^{(1)}\lambda^{(2)}}{\lambda^{(1)} + \lambda^{(2)}}(g^{(1)} - g^{(2)}). \tag{11}$$

The modelling of the effective mobilities $\lambda^{(l)}$, closing the model, is now considered.

3 NON PARAMETRIC MODEL UNCERTAINTY

The uncertainty in the model is assumed to arise from an incomplete knowledge of the effective mobilities only, since the principle of mass conservation expressed by Eq. (3) is unquestionable. It is then natural to consider these relations as random processes defined on an abstract probability space $(\mathcal{A}, \mathcal{F}, d\mu)$ and indexed by $s \in [0, 1]$. To make clear the distinction between random and deterministic quantities we shall use uppercase (resp. lowercase) letters to denote random (resp. deterministic) quantities.

3.1 Functional constraints

As stated before, $\Lambda^{(l)}$ are stochastic processes defined on $(\mathcal{A}, \mathcal{F}, d\mu)$, indexed by $s \in [0, 1]$ and taking value in $\mathbb{R}^+$. It is required that $\Lambda^{(1)}$ (resp. $\Lambda^{(2)}$) is increasing (resp. decreasing) with s and that it vanishes for $s = 0$ (resp. $s = 1$). Also, the saturated values of $\Lambda^{(1)}$ and $\Lambda^{(2)}$ (for $s = 1$ and $s = 0$ respectively) are known without uncertainty as they can be accurately measured in single-phase experiments. The saturated values will be simply denoted $\lambda_|^{(1)}$ and $\lambda_|^{(2)}$. Furthermore, it will be assumed that the effective mobilities are almost surely (a.s.) differentiable and convex functions of s. To summarize these functional assumptions, $\Lambda^{(1)}$ is such that

- $s \mapsto \Lambda^{(1)}(s)$ is a.s. continuous, increasing, differentiable and convex $\forall s \in [0, 1]$,
- $\Lambda^{(1)}(s = 0) = 0$ a.s.,

- $\Lambda^{(1)}(s=1) = \lambda_{|}^{(1)}$ a.s.,

while for $\Lambda^{(2)}$:

- $s \mapsto \Lambda^{(2)}(s)$ is a.s. continuous, decreasing, differentiable and convex $\forall s \in [0,1]$,
- $\Lambda^{(2)}(s=1) = 0$ a.s.,
- $\Lambda^{(2)}(s=0) = \lambda_{|}^{(2)}$ a.s..

It will be further assumed that the two stochastic processes are independent. In the following, we detail the construction of the probability law for $\Lambda = \Lambda^{(1)}$, the methodology for $\Lambda^{(2)}$ being essentially similar. We denote $V_{[0,1]}$ the space of continuous differentiable functions defined on $[0,1]$ such that

$$V_{[0,1]} \equiv \left\{ f : s \in [0,1] \mapsto \mathbb{R} \,\middle|\, \frac{df}{ds} \geq 0,\ \frac{d^2 f}{ds^2} \geq 0, f(0) = 0, f(1) = \lambda_{|} > 0 \right\}. \qquad (12)$$

3.2 Probabilistic constraints

We denote $p_\lambda(\lambda)$ the probability density function (pdf or density for short) of the stochastic process Λ. Clearly, $p_\lambda(\lambda) = 0$ for $\lambda \notin V_{[0,1]}$. Any functional $u : \Lambda \in V_{[0,1]} \mapsto \mathbb{R}$ is a random variable defined on $(\mathcal{A}, \mathcal{F}, d\mu)$ with expectation

$$E[u(\Lambda)] = \int_{\mathcal{A}} u(\Lambda(s,\omega)) d\mu(\omega) = \int_{V_{[0,1]}} u(\lambda) p_\lambda(\lambda) d\lambda,$$

where $\Lambda(s,\omega)$ denotes a realization of Λ. We define $u_1(\Lambda) \equiv \Lambda(0.5)$ and $u_2(\Lambda) = \Lambda^2(0.5)$, so that $E[u_1(\Lambda)]$ and $E[u_2(\Lambda)]$ are the first and second moments of the effective mobility at $s = 0.5$, denoted m_1 and m_2 respectively. Due to the functional properties of Λ, it is easy to show that :

$$m_1 \in [0, \lambda_{|}/2], \quad m_2 \in [m_1^2, m_1 \lambda_{|}/2]. \qquad (13)$$

In the following, m_1 and m_2 are prescribed -satisfying Eqs. (13)- and used to control the stochastic process Λ : m_1 controls the mean of the effective mobility while m_2 controls its variability, decaying as m_2 goes to m_1^2. In fact, we have to determine the density of Λ for given m_1 and m_2, *i.e.* $p_\lambda(\lambda; m_1, m_2)$. However, to simplify the notations, the dependence of the probability density function with the prescribed first and second moments will not be mentioned explicitly.

3.3 Maximum entropy principle

There is in general an infinite number of densities p_λ yielding the prescribed moments m_1 and m_2. An additional requirement is necessary to ensure uniqueness; specifically, we

want the the probability density function which is the least informative, *i.e.* the density maximizing the entropy[8]

$$\mathcal{S}(p_\lambda) = -\int_{V_{[0,1]}} p_\lambda \log p_\lambda d\lambda,$$

while satisfying the constraints :

$$\int_{V_{[0,1]}} p_\lambda(\lambda) d\lambda = 1, \tag{14}$$

$$\int_{V_{[0,1]}} u_1(\lambda) p_\lambda(\lambda) d\lambda = m_1, \tag{15}$$

$$\int_{V_{[0,1]}} u_2(\lambda) p_\lambda(\lambda) d\lambda = m_2. \tag{16}$$

This density is solution of a constrained optimization problem with Lagrangian

$$\begin{aligned}\mathcal{L}(p_\lambda, \beta_0, \beta_1, \beta_2) &= -\int_{V_{[0,1]}} p_\lambda \log(p_\lambda) d\lambda + (\beta_0 - 1)\left[1 - \int_{V_{[0,1]}} p_\lambda d\lambda\right] \\ &+ \beta_1\left[m_1 - \int_{V_{[0,1]}} u_1 p_\lambda d\lambda\right] + \beta_2\left[m_2 - \int_{V_{[0,1]}} u_2 p_\lambda d\lambda\right],\end{aligned} \tag{17}$$

where $\beta_{0,\ldots,2}$ are the Lagrange multipliers associated to the constraints in Eqs. (14-16). The stationarity of the Lagrangian with regard to the density p_λ leads to

$$p_\lambda(\lambda) = \exp\left[-\beta_0 - \beta_1 u_1(\lambda) - \beta_2 u_2(\lambda)\right]. \tag{18}$$

Replacing the last expression of p_λ in Eqs. (14-16) gives the (non-linear) equations for the Lagrange multipliers. To solve these equations, integrations over $V_{[0,1]}$ are required but the dimension of $V_{[0,1]}$ is infinite : a discretization of Λ in necessary to approach the problem in a finite dimensional space.

4 DISCRETIZATION OF THE PROCESS

4.1 Spline approximation

Let $0 = s_0 < s_1 < \ldots < s_n = 1$, be a set of points evenly distributed on $[0, 1]$ with step size $\delta = 1/n$: $s_i = i\delta$, for $i = 0, \ldots, n$. Let $\boldsymbol{W} \equiv (W_1, \ldots, W_n)$ be a random vector defined on $(\mathcal{A}, \mathcal{F}, \mu)$ with value in $W^n \subset (\mathbb{R}^+)^n$ such that

$$W^n = \left\{ \boldsymbol{W} \in (\mathbb{R}^+)^n \,\middle|\, \sum_{i=1}^{n} (n + 1 - i) W_i = \lambda_| \right\}. \tag{19}$$

We denote Λ_i the stochastic process value at $s = s_i$. Then, setting for $\boldsymbol{W} \in W^n$

$$\Lambda_0 = 0, \quad \Lambda_i = \lambda_| \left(\sum_{j=1}^{i} (i+1-j) W_j \right) \text{ for } i = 1, \ldots, n, \tag{20}$$

we have :

- $\Lambda(0) = 0$ a.s.;
- $\Lambda_i - \Lambda_{i-1} \geq 0$ a.s. for $i = 1, \ldots, n$ (increasing process);
- $\Lambda_{i+1} - 2\Lambda_i + \Lambda_{i-1} \geq 0$ a.s. for $i = 1, \ldots, n-1$ (convexity);
- $\Lambda_n = \Lambda(1) = \lambda_|$ a.s. (termination condition).

At this point, we have expressed the process values at a finite number of points s_i in terms of a finite dimensional random vector. These process values are consistent with the monotonicity, convexity and termination conditions. To complete the approximation of Λ for any $s \in [0,1]$ we rely on a shape preserving quadratic spline interpolation[9] between the data points $(s_i, \Lambda_i)_{i=0,\ldots,n}$. This interpolation scheme preserves the monotonicity and convexity of the data and yields continuous first order derivatives. It remains to determine the density of the finite dimensional vector $\boldsymbol{W}$.

4.2 Determination of the Lagrange multipliers

We denote $p_{\mathbf{W}}$ the probability density function of $\boldsymbol{W}$ and $u_{0.5}(\boldsymbol{W})$ the spline value of Λ at $s = 0.5$. The Eqs. (14-16) become :

$$\int_{W^n} p_{\mathbf{W}}(\boldsymbol{w}; \boldsymbol{\beta}) d\boldsymbol{w} = 1, \tag{21}$$

$$\int_{W^n} u_{0.5}(\boldsymbol{w}) p_{\mathbf{W}}(\boldsymbol{w}; \boldsymbol{\beta}) d\boldsymbol{w} = m_1, \tag{22}$$

$$\int_{W^n} u_{0.5}^2(\boldsymbol{w}) p_{\mathbf{W}}(\boldsymbol{w}; \boldsymbol{\beta}) d\boldsymbol{w} = m_2, \tag{23}$$

where the density of $\boldsymbol{W}$ is now

$$p_{\mathbf{W}}(\boldsymbol{w}; \boldsymbol{\beta}) = \exp[-\beta_0 - \beta_1 u_{0.5}(\boldsymbol{w}) - \beta_2 u_{0.5}^2(\boldsymbol{w})].$$

Here, we have made explicit the dependence of $p_{\mathbf{W}}$ with regard to the vector of Lagrange multipliers $\boldsymbol{\beta} = (\beta_0, \ldots, \beta_2)$. We propose the following iterative algorithm for the computation of the Lagrange multipliers.

1. Set $\boldsymbol{\beta}^{(0)}$ to an initial guessed value and iteration index k to zero.

2. Draw a sample $\{\boldsymbol{w}_l, l = 1, \ldots, m\}$ from $p_{\mathbf{W}}(\boldsymbol{w}, \boldsymbol{\beta}^{(k)})$. A numerical procedure to generate such sample is detailed in the next paragraph.

3. Compute a new estimate $\boldsymbol{\beta}^{(k+1)}$ of $\boldsymbol{\beta}$ solution of Eqs. (21-23), where the expectations are substituted with their Monte Carlo approximations based on the current sample :

$$\frac{1}{m}\sum_{i=1}^{m}\frac{p_{\mathbf{W}}(\boldsymbol{w}_i;\boldsymbol{\beta}^{(k+1)})}{p_{\mathbf{W}}(\boldsymbol{w}_i;\boldsymbol{\beta}^{(k)})} - 1 = 0, \tag{24}$$

$$\frac{1}{m}\sum_{i=1}^{m} u_{0.5}(\boldsymbol{w}_i)\frac{p_{\mathbf{W}}(\boldsymbol{w}_i;\boldsymbol{\beta}^{(k+1)})}{p_{\mathbf{W}}(\boldsymbol{w}_i;\boldsymbol{\beta}^{(k)})} - m_1 = 0, \tag{25}$$

$$\frac{1}{m}\sum_{i=1}^{m} u^2_{0.5}(\boldsymbol{w}_i)\frac{p_{\mathbf{W}}(\boldsymbol{w}_i;\boldsymbol{\beta}^{(k+1)})}{p_{\mathbf{W}}(\boldsymbol{w}_i;\boldsymbol{\beta}^{(k)})} - m_2 = 0. \tag{26}$$

4. Repeat from step 2 for the next iteration of the algorithm.

Efficient non-linear solvers, *e.g.* Newton-Raphson iterations, can be used to solve the equations at step 3 : derivation of the equations with regard to the unknown $\boldsymbol{\beta}^{(k+1)}$ is straightforward. Note also that during non-linear iterations, only the densities of the sample points $\boldsymbol{w}_i$ need to be updated, since $u_{0.5}(\boldsymbol{w}_i)$ and sampling densities $p_{\mathbf{W}}(\boldsymbol{w}_i;\boldsymbol{\beta}^{(k)})$ are left unchanged.

Because the estimates of $\boldsymbol{\beta}$ are based on randomly generated samples, they are random estimates with inherent variability. Consequently, the sequence of $\boldsymbol{\beta}^{(k)}$ is not expected to converge as $k \to +\infty$ for finite samples size m. On the contrary, the averages, $\widehat{\boldsymbol{\beta}^{(k)}}$, of successive estimates is expected to converge, at least for reasonable initial guessed value $\boldsymbol{\beta}^{(0)}$ and sufficiently large samples size m :

$$\boldsymbol{\beta} = \lim_{k\to+\infty}\widehat{\boldsymbol{\beta}^{(k)}}, \quad \widehat{\boldsymbol{\beta}^{(k)}} = \frac{1}{k}\sum_{j=1}^{k}\boldsymbol{\beta}^{(j)}. \tag{27}$$

In practice, the convergence of $\widehat{\boldsymbol{\beta}^{(k)}}$ is monitored during the iterations which are stopped when estimated relative variances of its components are all less than 1%.

4.3 Markov Chain Monte Carlo sampling

The main ingredient of the algorithm proposed in the previous paragraph is the sampling of W^n from the density $p_{\mathbf{W}}(\boldsymbol{w};\boldsymbol{\beta}^{(k)})$. To this end, a particular Markov Chain Monte Carlo[10] (MCMC) sampler, known as the hit-and-run algorithm[11] is used. This MCMC sampler is designed to yield a sequence of dependent sample points $\{\boldsymbol{w}_l, l = 1, \ldots, m\}$ converging (in distribution) to $\boldsymbol{W} \sim p_{\mathbf{W}}(\boldsymbol{w};\boldsymbol{\beta}^{(k)})$.

To construct this algorithm, it is first remarked that the admissible space W^n is a bounded portion of an hyperplane Π of $\mathbb{R}^n$. Boundaries of W^n are the intersections of Π

with the n hyperplanes $\Pi_{i=1,\ldots,n}$ having for equations $w_i = 0$. A direction normal to Π is $\boldsymbol{c} \equiv (c_1, \ldots, c_n)$, the vector of $\mathbb{R}^n$ with components $c_{i=1,\ldots,n} = n + 1 - i$. We denote $\boldsymbol{c}'$ the unitary vector normal to Π : $\boldsymbol{c}' \equiv \boldsymbol{c}/\|\boldsymbol{c}\|$. The situation is schematically illustrated for $n = 3$ in the left plot of Figure 1.

Since sample points are in W^n, it is obvious that $(\boldsymbol{w}_{l+1} - \boldsymbol{w}_l) \cdot \boldsymbol{c}' = 0$; in other words the "move" between two successive sample points is parallel to Π. This suggests to sample W^n using displacements in Π along random directions orthogonal to $\boldsymbol{c}$. To sample the direction parallel to Π, let $\boldsymbol{\delta}_l$ be a vector of $\mathbb{R}^n$ drawn at random with independent identically distributed components (for instance normalized Gaussian distributions). This vector can be decomposed in terms of a vector $\boldsymbol{\delta}_l^{\parallel}$ parallel to Π and a vector $\boldsymbol{\delta}_l^{\perp}$ orthogonal to $\boldsymbol{c}'$,

$$\boldsymbol{\delta}_l = \boldsymbol{\delta}_l^{\parallel} + \boldsymbol{\delta}_l^{\perp}, \quad \boldsymbol{\delta}_l^{\perp} \equiv (\boldsymbol{\delta}_l \cdot \boldsymbol{c}')\boldsymbol{c}'.$$

We define $\boldsymbol{w}^*(r) = \boldsymbol{w}_l + r\boldsymbol{\delta}_l^{\parallel}$.

For $\boldsymbol{w}^*(r) \in W^n$ it is necessary that $r^- \leq r \leq r^+$ as illustrated in the middle plot of Figure 1. Consequently, $\boldsymbol{w}_{l+1}$ will be constructed by sampling a scalar $r_l \in [r^-, r^+]$ from the density $f(r) \propto p_{\mathbf{W}}(\boldsymbol{w}_l + r\boldsymbol{\delta}_l^{\parallel}; \boldsymbol{\beta}^{(k)})$ and setting $\boldsymbol{w}_{l+1} = \boldsymbol{w}_l + r_l\boldsymbol{\delta}_l^{\parallel}$. Because $f(r)$ is univariate, it can be easily sampled.

As mentioned previously, repetitions of the hit-and-run iteration yields successive sample points $\boldsymbol{w}_l$ that converge in probability to $\boldsymbol{W} \sim p_{\mathbf{W}}(\boldsymbol{w}; \boldsymbol{\beta}^{(k)})$. However, the convergence rate of the sequence to the stationary distribution $p_{\mathbf{W}}$ is finite so that the first m' iterates should be disregarded and the total length of the simulated Markov Chain is $m + m'$. Determination of the length of burn-in m' is not an easy task even-though criteria can be found in the literature. However, for the application of the hit-and-run algorithm considered in this work, we do not expect the successive iterates $\boldsymbol{\beta}^{(k)}$ of the Lagrange multipliers to be significantly different from an iteration to the next one, but to fluctuate because of sampling error only, as $k \to \infty$. As a consequence, if m is large enough, changes in the sampling density should be small too, such that taking at random a sample point $\boldsymbol{w}_l$ of the Markov Chain based on $\boldsymbol{\beta}^{(k)}$ as initial sample point $\boldsymbol{w}_0$ of the following chain to be constructed with $\boldsymbol{\beta}^{(k+1)}$, significantly reduce the burn-in length. In the numerical examples presented below, the burn-in length m' was varied from a few hundreds ($n = 4$) to a few thousands ($n = 32$). The dimension m of the sample has also to be increased with the dimension n of the discretization space; we have used $m = 10^4 n$ to ensure a sufficient excursion of W^n.

4.4 Numerical examples

In this paragraph, we present examples of the construction of a discretized random process $\Lambda(s)$ with $\lambda_| = 1$ and $m_1 = 0.2$. The second parameter, m_2, is selected to yield a standard deviation of Λ at $s = 0.5$ equal to 0.025.

The convergence of the stochastic process for increasing discretization space W^n, $n = 4$, 8, 16 and 32, is first investigated. Results are reported in Figure 2, where plotted are

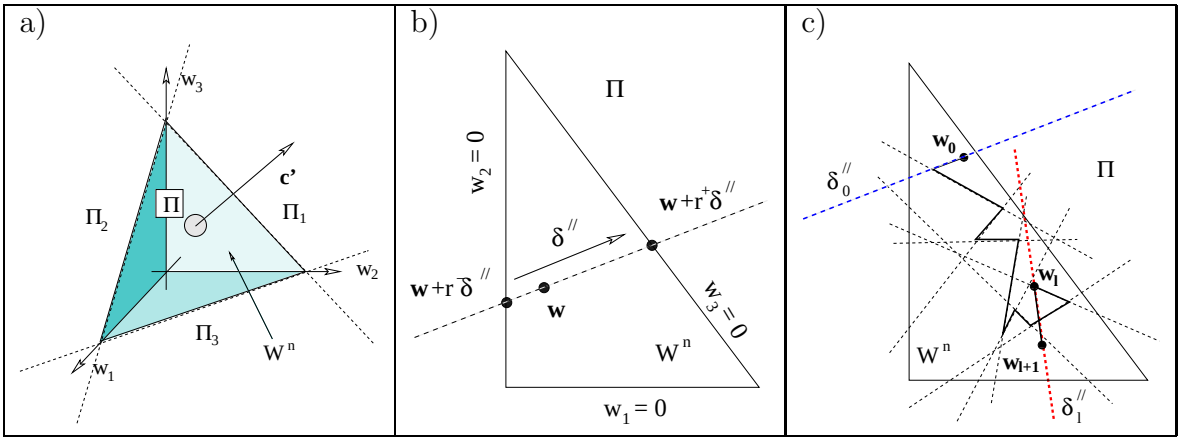

Figure 1: Illustration of the hit-and-run sampling algorithm for $n = 3$. a) Representation of the sampling domain W^n as a portion of the plane Π with normal $\boldsymbol{c}'$ and bounded by the planes $\Pi_{i=1,2,3}$. b) Illustration of the possible move from a point $\boldsymbol{w}$ along a direction $\boldsymbol{\delta}^{\|}$ parallel to Π : the move is limited to $r^{\pm}\boldsymbol{\delta}^{\|}$ in order to remain in W^n. c) Representation of successive hit-and-run iterations : the displacement from $\boldsymbol{w}_l$ to $\boldsymbol{w}_{l+1}$ is $r_l\boldsymbol{\delta}_l^{\|}$ where $r_l \in [r_l^-, r_l^+]$ is drawn at random from $f(r) \propto p_{\mathbf{W}}(\boldsymbol{w}_l + r\boldsymbol{\delta}_l^{\|}; \boldsymbol{\beta}^{(k)})$.

20 realizations $\Lambda(s;\omega)$ drawn at random from the computed probability density functions and, to ease the comparison between different n, the usual ± 3 standard deviations bounds centered on the respective expectations $E[\Lambda(s)]$. These results highlight the quick convergence of $E[\Lambda]$ with n : expectations are virtually equal for $n \geq 8$. On the contrary, the convergence of the variance of $\Lambda(s)$ is much slower with n. Specifically, for $n = 4$ and 8 the variances present a local minimum (a node) at $s = 0.5$ which is not present for larger n. Since the variance of Λ at $s = 0.5$ is the same in every cases, the node has for origin an over-estimation of the actual variability of the process at $s \neq 1/2$ and small n. This effect can be attributed to a lack of degrees of freedom in the stochastic model to properly account for the dependencies in Λ between different index values s.

Figure 3 reports, for $n = 32$, the convergence of the averages $\widehat{\beta_1^{(k)}}$ and $\widehat{\beta_2^{(k)}}$ with the iteration index k of the computational algorithm described in paragraph 4.2. The curves show that, after some iterations along which $\widehat{\boldsymbol{\beta}^{(k)}}$ significantly evolves, denoting the influence of the initial guessed value $\boldsymbol{\beta}^{(0)}$, it ends oscillating with fluctuations having decaying amplitude (note the log-scale in iteration index). As explained previously, these fluctuations are due to the finite size of the samples used in the computation, that induces randomness in the successive estimates of $\boldsymbol{\beta}^{(k)}$. However, when averaged, these stochastic fluctuations cancel as shown in Figure 4 where plotted are Monte Carlo estimations of the standard deviations of $\widehat{\beta_1^{(k)}}$ and $\widehat{\beta_2^{(k)}}$ as a function of the iteration index k. As one may have expected, the standard deviations of the averages $\widehat{\boldsymbol{\beta}^{(k)}}$ decay with a $1/\sqrt{k}$ rate, demonstrating the convergence of the algorithm.

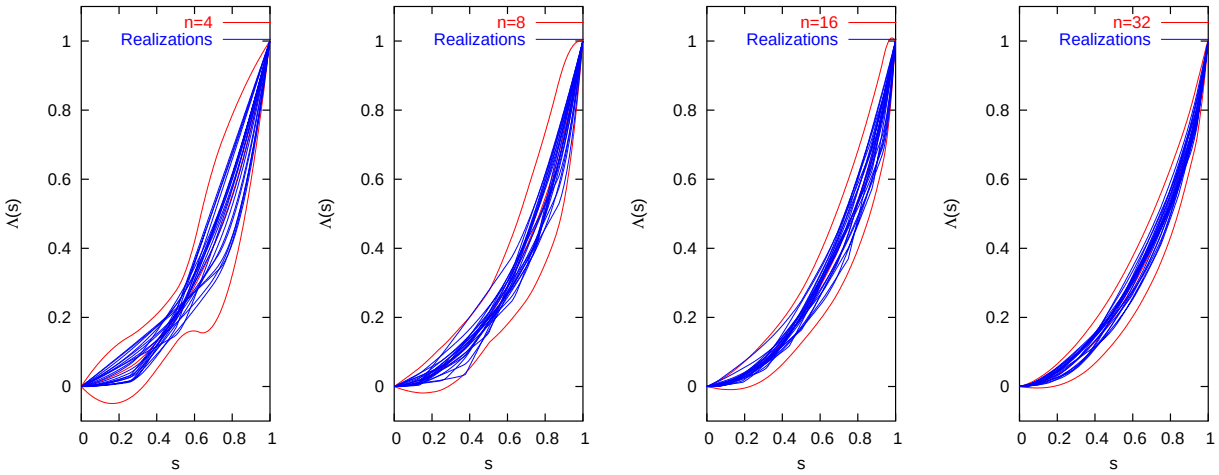

Figure 2: Convergence of the approximated stochastic process $\Lambda(s)$ as n increases : $n = 4$, 8, 16 and 32 (from left to right). Plots show a sample of 20 random realizations $\Lambda(s;\omega)$ and the $\pm$ 3 standard deviations bounds centered on $E[\Lambda(s)]$. The process is characterized by $m_1 = 0.2$, $m_2 = 0.040625$ and $\lambda_| = 1$.

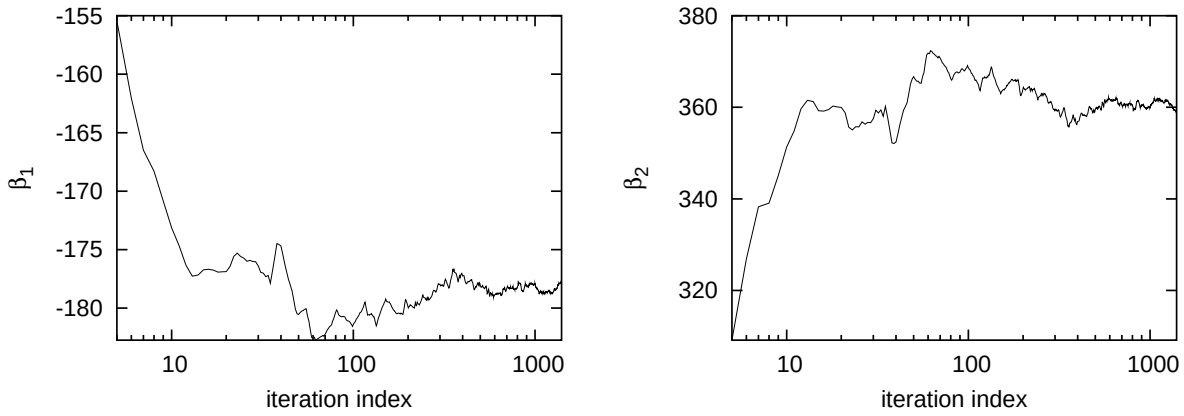

Figure 3: Convergences of the averages of the Lagrange multipliers $\widehat{\beta_1^{(k)}}$ (right) and $\widehat{\beta_2^{(k)}}$ (left)with the iteration index k. The process is characterized by $m_1 = 0.2$, $m_2 = 0.04025$ and $\lambda_| = 1$. The discretization uses $n = 32$.

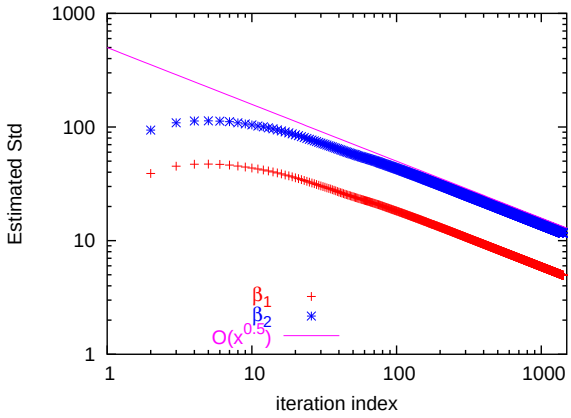

Figure 4: Convergences the estimated variances in $\widehat{\beta_1^{(k)}}$ and $\widehat{\beta_2^{(k)}}$ as a function the iteration index k. The solid line corresponds to a decay rate of $1/\sqrt{k}$. The process is characterized by $m_1 = 0.2$, $m_2 = 0.04025$ and $\lambda_| = 1$. The discretization uses $n = 32$.

5 ANALYSIS OF MODEL UNCERTAINTY

5.1 Test flow and uncertainty model

The impact of model uncertainty on the two-phase flow is now investigated for the separation by gravity of two phases with different densities, in a vertical (align with gravity) column with normalized height $L = 2$ ($\Omega = [-1, 1]$) and porosity $\phi = 0.9$. The normalized gravity terms are set to $g_1 = 1$ and $g_2 = 0.7$. At $t = 0$, the two fluids are well mixed ($s = 0.5$) then the gravity separates the phases as the heavy fluid (phase 1) flows downward while the light fluid (phase 2) flows upward. The boundary conditions for this problem are no-flux across the boundaries ($z = \pm 1$). The discretization used a time step $\Delta t = 0.025$ and $N_z = 400$ cells. The asymptotic solution for $t \to +\infty$ is $s = 0$ for $z > 0$ and $s = 1$ for $z < 0$. This behavior is illustrated in Figure 5.

The effective mobilities have known termination conditions at $s = 0$ and $s = 1$, as discussed in section 3. Specifically, we set $\lambda_|^{(1)} = 1$ and $\lambda_|^{(2)} = 1.43$. The random constitutive relations $\Lambda^{(1)}$ and $\Lambda^{(2)}$ are independent and parametrized by their first and second moments at $s = 0.5$. We write these moments as

$$m_1^{(l)} = \alpha \lambda_|^{(l)}, \quad m_2^{(l)} = (1 + \gamma^2) \left(m_1^{(l)} \right)^2 \quad l = 1, 2.$$

For this setting, the two effective mobilities have expectations at $s = 0.5$ equal to the same fraction α of their respective maximum $\lambda_|^{(l)}$ and equal relative level of variability (coefficient of variation) controlled by γ^2. As a consequence, $\Lambda^{(1)}(s)/\lambda_|^{(1)}$ and $\Lambda^{(2)}(1 - s)/\lambda_|^{(2)}$ are equivalent stochastic processes. Moreover, provided that the two effective mobilities are approximated on the same finite dimensional space W^n, one has to solve a unique optimization problem, using the methodology described in the previous section,

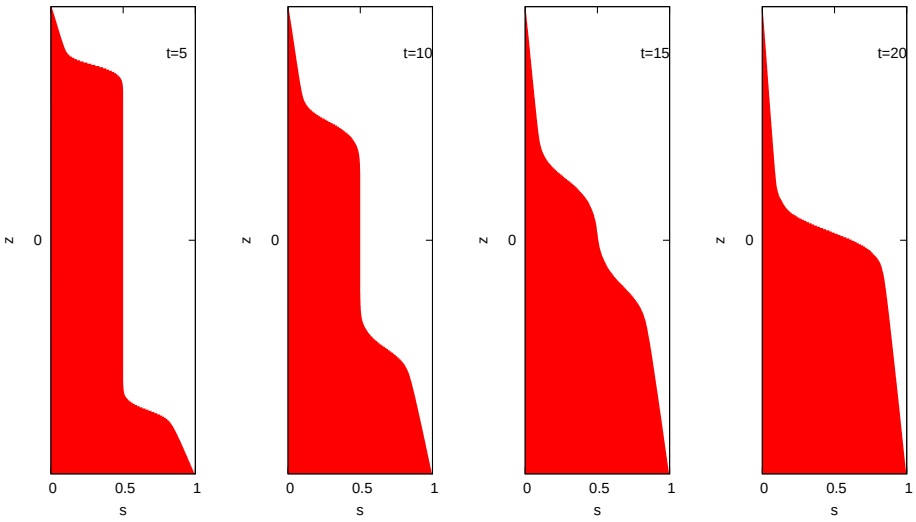

Figure 5: Deterministic solution at different times t as indicated of the two-phase flow problem as defined in section 5. The constitutive relations used in this simulations are the expectations of $\Lambda^{(1)}$ and $\Lambda^{(2)}$ for $\alpha = 0.2$, $\gamma = 0.025$ and $n = 32$.

for $m_1 = \alpha$, $m_2 = (1+\gamma^2)\alpha^2$ and $\lambda_| = 1$. The effective mobility $\Lambda^{(1)}$ and $\Lambda^{(2)}$ are then simply deduced from $\Lambda(s)$ by means of a rescaling by $\lambda_|^{(l)}$ and a change of variable $s \to (1-s)$ for $\Lambda^{(2)}$. In fact, when the process $\Lambda(s)$ is determined, two independent hit-and-run Markov chains are run, yielding samples of $\Lambda^{(1)}$ and $\Lambda^{(2)}$. To improve further the mixing of the chains, sample points of the effective mobilities are recorded every 10,000 hit-and-run iterations of the MCMC algorithm. This procedure yields a sample of the effective mobilities (*i.e.* of the random model)

$$M \equiv \{(\Lambda^{(1)}(s;\omega_i), \Lambda^{(2)}(s;\omega_i)), i = 1, \ldots, q\}.$$

Then, for each realizations of the effective mobilities in the sample M, the deterministic equations of the flow are solved yielding realizations of the solution of the random model. This set of realizations $\{S(z,t;\omega_i), i = 1, \ldots, q\}$ can be used in turn to estimate the probability law of the flow (*e.g.* moments, quartiles, correlations, ...) as shown below. In the following numerical examples, the sample size is fixed to $q = 2,500$.

5.2 Convergence of the random flow with discretization

We set $\alpha = 0.2$ and $\gamma = 0.025$ and we analyze the convergence of $S(z,t)$ as the discretization of the effective mobilities is refined from $n = 4$ to $n = 32$. Figure 6 presents the MC sample mean of $S(z,t)$ at $t = 5$, 10, 15 and 20 for different discretizations using $n = 4$, 8, 18 and 32. It is found that the sample mean indeed converges with n. However, noticeable differences are reported for $n = 4$ and $n = 8$. These differences are essentially due to the over-estimation of the variability of the effective mobilities for small values of n as shown in section 4 : because the flow is non-linear, the mean solution depends on the

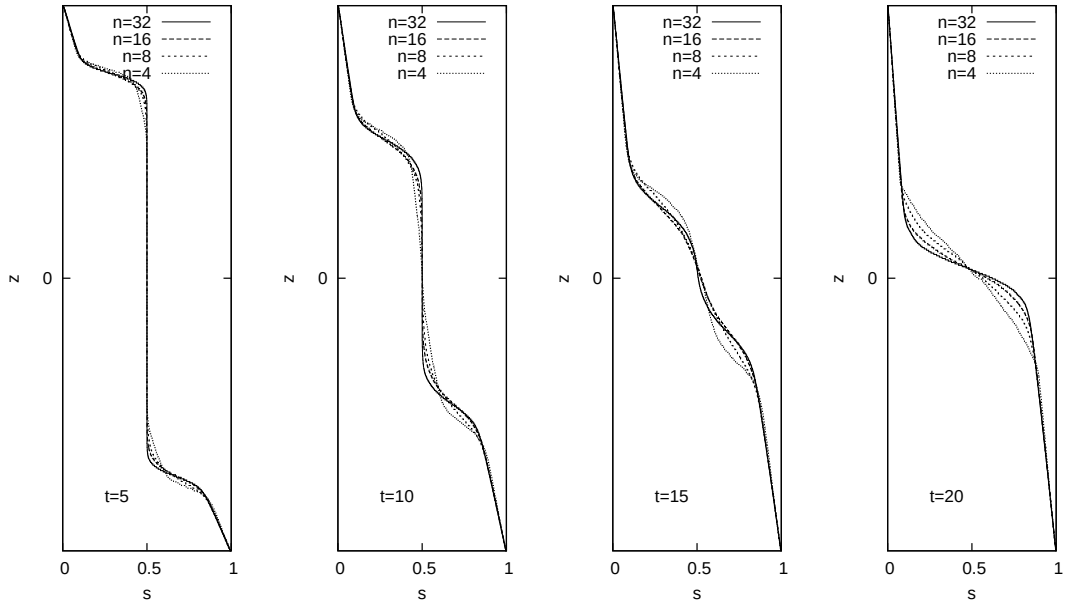

Figure 6: Convergence with the discretization parameter n of the sample mean of $S(t,z)$ for a fixed random model ($\alpha = 0.2$ and $\gamma = 0.025$). Plots show the expectations of S at different times as indicated.

model variability even if the mean model (expected mobilities) is essentially independent of n. In fact, the differences with n of the sample mean can be attributed to a larger dispersion of the characteristic flow time-scale for small n.

Figure 6 presents for $n = 4$, 8, 16 and 32 the resulting variability in the random solution in terms of the sample mean with $\pm$ 3 standard deviation bounds at $t = 10$ (top line) and $t = 20$ (bottom line). Again, the plots show that the discretized model tends to over-estimates the variability of the solution for small n. This trend is consistent with the findings of section 4 as a larger dispersion of the effective mobilities reasonably induces a larger dispersion of the model solution. It is also found that the uncertainty in S is larger where the mean solution presents significant gradients.

5.3 Impact of mean model

The impact of the parameter α of the random model is now investigated, for fixed relative variability $\gamma = 0.025$. Roughly speaking, this is equivalent to compare the random solutions corresponding to random models with different means but constant variability. Figure 8 depicts the sample means of $S(z,t)$ with $\pm$ 3 standard deviation bounds for two random models using $\alpha = 0.2$ and $\alpha = 0.3$. The two simulations use $n = 32$. The results show that the main impact of the selected mean model is on the mean characteristic time scale of the flow : the separation speed of the two phases is larger for $\alpha = 0.3$ than for $\alpha = 0.2$. On the contrary, the variability of the solution seems to be much less affected by the selected mean model. However, a proper time rescaling of the solutions would be

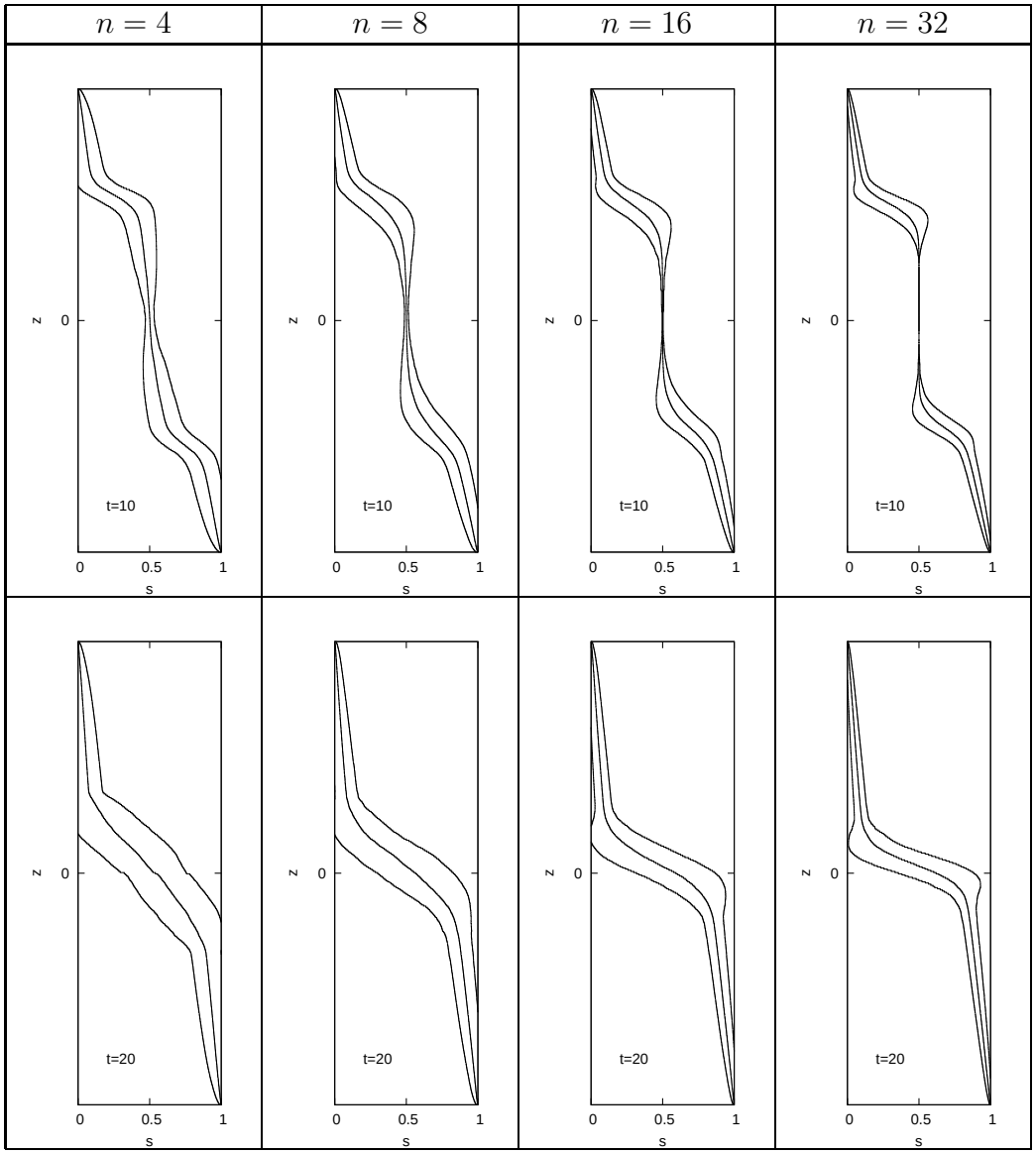

Figure 7: Convergence with the discretization parameter n of the random solution $S(z,t)$ at $t = 10$ (top line) and $t = 20$ bottom lines. Plots show the sample mean of $S(t,z)$ with $\pm$ 3 standard deviation bounds. The random models are characterized by $\alpha = 0.2$ and $\gamma = 0.025$.

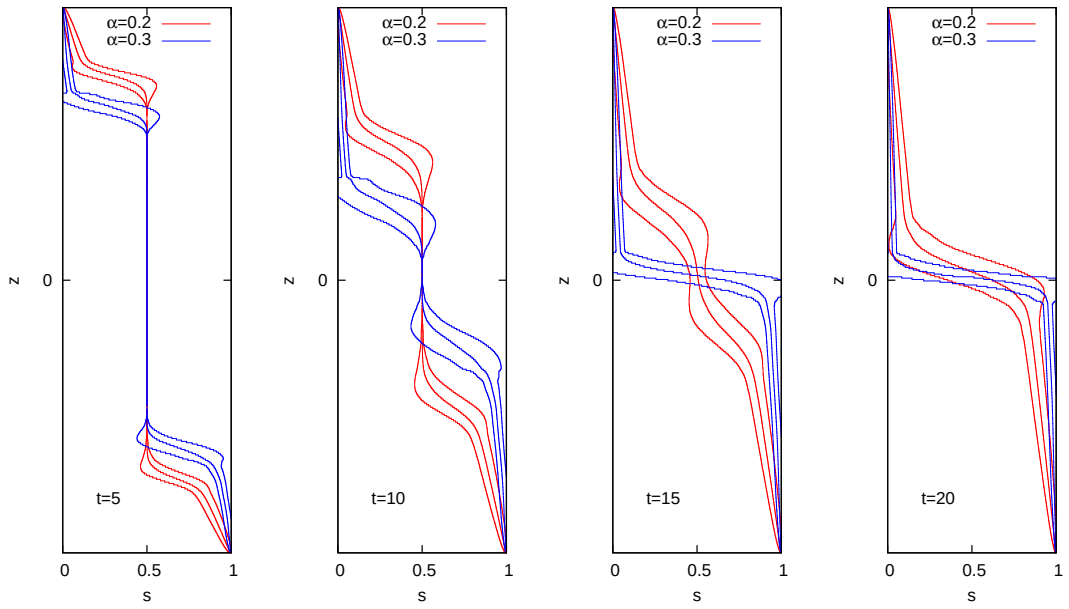

Figure 8: Comparison at different times of the sample means with ± 3 standard deviation bounds of the random solutions $S(z,t)$ for two uncertain models with different means corresponding to $\alpha = 0.2$ and 0.3. The relative variability of the two models is equal and given by $\gamma = 0.025$. Random models are discretized using $n = 32$.

necessary for a finer comparison of the variability.

5.4 Impact of model variability

Finally, in a last numerical experiment, we set $\alpha = 0.2$ and we vary γ. This experiment corresponds roughly to a constant mean model with increasing variability. We used $\gamma = 0.015$, 0.025 and 0.05 and a discretization with $n = 16$. The results are summarized in Figure 9 where plotted are the sample means of $S(t,z)$ with ± 3 standard deviation bounds at times $t = 5$, 10, 15 and 20. As expected, a larger variability of the model induces a larger variability of the solution. Also, the influence of the model variability on the mean solution is clearly visible. Again this is essentially explained by the non-linearity of the flow as the mean model is weakly affected by the value of γ. In fact, it is found that a larger value of γ leads to a smoother profile $E[S(t,z)]$ at a given time. This trend denotes an increased dispersion of the characteristic time-scale of the flow as γ increases.

6 CONCLUSION

A non parametric approach has been proposed for the analysis of model uncertainty in two-phase flow through a porous medium. The stochastic flow model is constructed using the maximum entropy principle on the basis of the available information regarding the effective mobilities of the phases (functional and probabilistic constraints).

The discretization of the effective mobilities leads to the resolution of an optimiza-

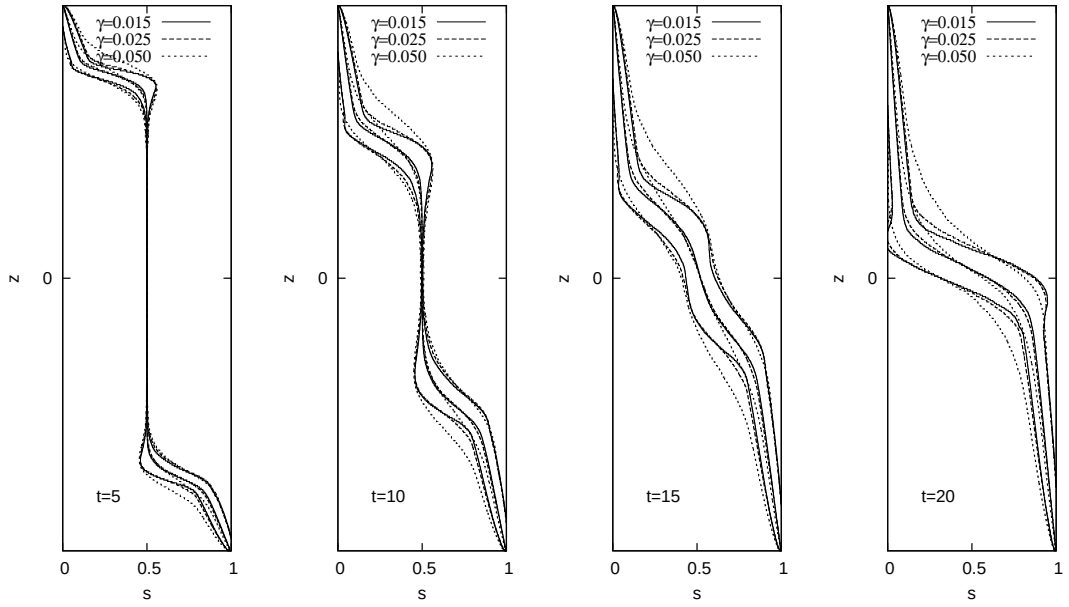

Figure 9: Comparison at different times of the sample means with $\pm$ 3 standard deviation bounds of the random solution $S(z,t)$ for uncertain models with increasing relative variability : $\gamma = 0.015$, 0.025 and 0.050. The three models have similar means given by ($\alpha = 0.2$). Random models are discretized using $n = 16$.

tion problem for the probability density function of a finite dimensional random vector. Resolution of this optimization problem allows for the sampling of the effective mobilities yielding realizations of the random model and corresponding realizations of the flow. Then, a Monte Carlo simulation technique can be used to estimate the probability law of the flow. Numerical examples have shown the effectiveness of the methodology in estimating the resulting characteristics of the random flow depending on the assumed characteristics of the random model (the value of the mean model and its variability at $s = 0.5$).

However, some aspects of the proposed methodology need further investigations :

- The convergence of the random effective mobilities with the discretization parameter n should be improved to avoid the difficulties associated with high-dimensional sampling. Here, a different discretization strategy may be a solution.

- The characteristics of the random model are parametrized by the expectations and variances of the effective mobilities at $s = 0.5$, the two constitutive equations being assumed independent. This may be too restrictive and arbitrary. In fact, we believe that the random model should account for the random solvability constraint :

$$E\left[\left(\max_{s\in[0,1]} \frac{1}{[\Lambda^{(1)}(s) + \Lambda^{(2)}(s)]}\right)^2\right] = \zeta < +\infty.$$

The random models presented in this paper indeed satisfy the solvability constraint, but it is not controlled. Substituting the solvability constraint to Eq. (16) would lead to a theoretically better grounded random models with a unique parameter ζ controlling the model variability. However, it will render the two constitutive relations dependent with a joined density $p(\lambda^{(1)}, \lambda^{(2)})$ to be computed.

- The physical model of the flow should be complemented to account for instance of capillarity forces, by means of an additional random process $P_c(s)$.

On-going work is focusing on these aspects.

REFERENCES

[1] O. Knio and O. Le Maître, Uncertainty Propagation in CFD Using Polynomial Chaos Decompositions, *Fluid Dynamics Research*, (in press).

[2] R.G. Ghanem and P.D. Spanos, *Stochastic Finite Elements: A Spectral Approach*, Springer Verlag, (1991)

[3] O.P. Le Maître, O.M. Knio, H.M. Najm and R.G. Ghanem, A stochastic projection method for fluid flow. I. Basic formulation, *J.* Computational Physics **173**(2), pp. 481-511, (2001).

[4] O.P. Le Maître, M.T. Reagan, O.M. knio, H.N. Najm and R.G. Ghanem, A stochastic projection method for fluid flow. II. Random Process, *J.* Computational Physics, **181**(1), pp. 9-44, (2002).

[5] D. Xiu and G.E. Karniadakis, Modeling Uncertainty in flow simulation via generalized Polynomial chaos, *J. Comput. Physics*, **187**, pp. 137–167, (2003).

[6] C. Soize, Random matrix therory for modeling uncertainties in computational mechanics, *Comput. Methods Appl. Mech. Eng.*, **(194)**, pp. 1333–1366, (2005).

[7] J. Jaffré, Flux calculation at the interface between two rock types for two-phase flow in porous media, *Technical Report n^o. 2075*, INRIA, (1993).

[8] E.T. Jaynes, Information theory and statistical mechanics, *Physical review*, **106**(4), pp. 620–630, (1957).

[9] D.F. McAllister and J.A. Roulier, Algorithm 574 : Shape preserving osculatory quadratic splines, *ACM Transactions on Mathematical Software*, **(7)**-3, pp. 384–386, (1981).

[10] W.R. Gilks, S. Richardson and D.J. Spielgelhalter, *Markov Chain Monte Carlo in Practice*, Chapman & Hall/CRC, London, (1998).

[11] M.-H. Chen and B.W. Schmeiser, General hit-and-run Monte-Carlo sampling for evaluating multidimensional integrals, *Operations Research Letters*,**19**-(4),pp. 161–169, (1996).